2022-01-1182 Published 19 Sep 2022

Chemical Characterization of Nanoparticle Emissions from Brakes - The nPETS Project

Alessandro Mancini, Bozhena Tsyupa, Matteo Federici, Mara Leonardi, Alessandro Piglione, Marco Bandiera, Andrea Bonfanti, and Federico Bertasi Brembo Spa

Citation: Mancini, A., Tsyupa, B., Federici, M., Leonardi, M. et al., "Chemical Characterization of Nanoparticle Emissions from Brakes - The nPETS Project," SAE Technical Paper 2022-01-1182, 2022, doi:10.4271/2022-01-1182.

Received: 25 May 2022 Revised: 21 Jul 2022 Accepted: 21 Jul 2022

Abstract

nPETS - nanoParticle Emissions from the Transport Sector - is an EU- funded project within the Horizon 2020 research and innovation program, with the aim of characterizing specifically the emission amount, the chemical composition and the toxicological behavior of nano-particulates produced by different exhaust and non-exhaust emission sources related to the transport sector. Started in June 2021, its final goal is to provide a wide scientific background for informed public health policies aiming to tackle transport-related nano-particulates, while developing sound technologies for their collection, chemical analysis and toxicological characterization. In particular, the chemical characterization of the collected nano-particulates is of fundamental importance in determining the presence of univocal markers for specific emission sources in different environments. Furthermore, it plays a pivotal role in explaining nano-emissions environmental and toxicological interactions, which will be studied during the second half of the project. With specific reference to the non-exhaust nano-particulates generated during braking operations, this paper summarizes the results obtained during the first period of project activities. More specifically, dedicated collection procedures, measurement protocols and physico-chemical characterization of brakes ultra-fine emissions are described and discussed. Notably, a comprehensive study of the chemical composition of brake emissions of nanometric dimensions is still lacking in literature. To this end, this paper reports for the first time a comparative assessment between the chemical composition of the brake emissions from nanometric dimensional fraction (d_{50} < 150 nm) with respect to those from coarser fractions.

1. Introduction

Air quality represents nowadays one of the main environmental concerns from the social, economic and political point of view [1, 2]. In the last decades, a vast scientific and technological effort has been deployed to monitor air pollutants and to improve the strategies necessary for their reduction. Notably, this effort has often found application in important legislation activities [3, 4]. However, in spite of all these efforts, air pollutants still represent a main concern affecting the life of people worldwide [2, 5, 6]. In particular, among all the categories of air pollutants, particulate matter (PM) is one of the pollutants that are least affected by the adopted countermeasures, showing at the same time strong effects on the human health, which are directly correlated to the size and chemical composition of the considered airborne particles [5, 6, 7, 8, 9, 10]. More adverse health effect are typically related to finer particulates, since they become progressively more bio-available and chemically reactive as their dimensions decrease and their specific areas increase [9].

A major fraction of outdoor airborne particulates, including the ultra-fine dimensional ranges, is generated from road, rail, air, and sea transportation. This becomes particularly evident in the urban environment. The transport sector alone generates approximatively 12% of the total PM_{10} and $PM_{2.5}$ produced by anthropogenic sources within the EU [2]. This percentage relates mainly to the road transport (10%), while the non-road counterpart constitutes a minor contribution (2%) [2]. As already reported, these figures can drastically increase when considering the urban environment (up to six times) [2]. However, no conclusive source apportionment studies are available for nanoparticle emissions. For all the reported reasons, the nPETS [11] EU-project consortium aims to improve the knowledge on transport-related nanoparticle emissions and their impacts on environment and health.

Looking more specifically at the road transport situation, particulates generated inside this category are typically divided in: *i)* exhaust emissions, when generated by internal combustion engines; and *ii)* non-exhaust emissions, when produced by others sources such as brakes, tyres, clutches together with resuspension effects. Nowadays, the two contribution are estimated to weigh in similar proportion. However, the non-exhaust fraction is expected to increase in the coming years due to the development of electric mobility [12, 13, 14]. Among non-exhaust sources, brakes are estimated to

contribute for 55% and 21% to the PM_{10} and $PM_{2.5}$ fractions, respectively [12, 13, 14]. However, studies involving the specific characterization of the ultra-fine dimensional fractions of emissions generated by brakes are substantially missing in the literature. Therefore, the investigation reported in this paper focuses on the first results obtained within the perimeter of activities of the nPETS project related to the investigation of nanoparticle emissions generated by brakes, and more in detail on their chemical characterization. In addition to the specific results of chemical composition of the brake emission ultra-fine fraction (d_{50} < 150 nm), a comparative assessment with results obtained for coarser fractions is also reported. Finally, a critical evaluation of the strategies adopted to optimize collection, manipulation and analysis of extremely limited amounts of sample in the form of nanoparticle powders is provided. The reported results will be used in the second half of the project, together with chemical evidences collected on other transport-related nanoparticle emissions, in order to investigate their ecological and toxicological behaviors as well as to perform accurate source apportionment studies.

TABLE 1 Nominal composition of BD and FM. Only elements with concentration higher than 0.1 wt% are reported for brevity.

BD		FM	
Element	**[wt%]**	**Element**	**[wt%]**
C	3.8	**C**	31.5
Si	1.9	**Fe**	23.8
Mn	0.5	**O**	14.8
Cu	0.2	**Zn**	6.1
Cr	0.1	**Mg**	5.5
Fe	*balance*	**Al**	4.1
Others	*traces*	**Sn**	3.9
		S	3.0
		Cr	2.3
		Si	2.2
		K	2.0
		Ca	0.4
		Cu	0.3
		Mn	0.1
		Others	*traces*

2. Experimental

The following paragraphs describe the materials and the analytical protocols adopted for sample collection and chemical characterization. Particular attention is devoted to the description of the procedures used to optimize the management of limited amounts of particles of nanometric dimensions.

2.1. Materials

Brake-related nanoparticle emissions are generated by a friction pair composed by a fully pearlitic gray cast iron braking disc (BD) coupled against an ECE R90 Copper-free friction material (FM). The nominal elemental composition of the materials involved in the study is reported in Table 1 for reference.

2.2. Samples Collection

The particulate samples are collected at a dyno-bench designed for emissions collection during tests performed in controlled conditions [15, 16]. The emission test procedure used to collect the particulates is the WLTP-Brake Cycle [17]: the PM material is collected both during the bedding cycles (5 WLTP-Brake repetitions) and during the cycle typically used for the evaluation of the emissions (*i.e.,* the 6th WLTP-Brake Cycle repetition) in order to maximize the amount of collected nanoparticles. For the same purpose, three repetitions of a single emission test are carried out, each repetition with new discs and pads. For all the tests, the braking corner is composed by: *i)* a four pistons fixed Aluminum caliper with pistons diameter of 44 mm; *ii)* a vented braking disc with a diameter of 342 mm and a thickness of 32 mm; and *iii)* a couple of pads with a surface of 89.1 cm^2. During the dyno-bench tests, a controlled particle-free air flux of 245 m^3 h^{-1} enters the brake enclosure in order to fulfill the temperature targets as suggested by the most recent guidelines from the Particle Measurement Programme (PMP) Informal Working Group [18] (a tailored calibration run is carried out before the bedding phases). The air flux is filtered through a HEPA-H13 filter which ensures an average filtration efficiency higher than 99.95%.

The collection of the PM emissions is carried out by an isokinetic sampling-probe, equipped with sharp-ended nozzles to ensure a high efficiency sampling. The airborne particles are sampled through two specific measurement instruments: a Dekati Electrical Low Pressure Impactor (ELPI+) and a Dekati Gravimetric Impactor (DGI). The ELPI+ allows real-time measurement of the size distribution and concentration of particles in the size range of 6 nm to 10 µm with a sampling rate of 10 Hz. For this study, the last five stages of the impactor are initially considered (d_{50} < 120 nm), employing polycarbonate filters. However, in spite of all the strategies adopted for the sampling, the amount of collected material on the lower stages of the ELPI+ resulted extremely low and thus insufficient for a reliable chemical characterization. In order to overcome this problem, material collected on the DGI collection substrates is used for chemical analysis. The DGI is a high sample flow rate cascade impactor able to collect particles in five size fractions below 2.5 µm. The instrument is used at the flow rate of 95 L/min and a cyclone with a 2.5 µm cutoff is placed before the inlet to provide the first dimensional cut. Greased aluminum substrates are used for the upper four stages, while a Teflon filter (pores diameter of 3 µm) is used as backup. In this paper, the material collected on the first collection substrate (**S1**: 130 < d_{50} < 150 nm) represents the target sample for the study of the nanoparticle emissions generated by brakes. This ultra-fine particulate is then compared with material collected on the higher collection substrates (**S2**: 400 < d_{50} < 450 nm; **S3**: 800 < d_{50} < 900 nm; **S4**: 2.1 < d_{50} < 2.2 µm).

One fourth of each collected substrate is used for chemical analysis, while the remaining material is spared for the eco/cyto-toxicological characterization, which will be performed in the second half of the project. The four investigated particulates are stripped from the collection substrates after dissolution of the collection grease in acetone and following sonication in 1 mL of isopropyl alcohol at 35 kHz for 2 minutes. The suspended particles are then recollected by centrifugation at 3000 rpm for 5 minutes and dried overnight in mild vacuum conditions (20 mbar) before the chemical analysis. The standalone powders are deposited on Aluminum stubs previously covered with carbon tape for electron microscopy. The particulates are always manipulated with a small metallic yet non-magnetic spatula and stocked or deposited in glass containers in order to minimize the potential loss of sample material.

2.3. SEM/EDXS Analysis

Scanning Electron Microscopy (SEM) imaging is used in order to verify qualitatively the granulometric profiles of the collected particulates. Energy Dispersive Spectroscopy (EDXS) analysis is coupled with the SEM probe in order to perform a comparative assessment of the elemental compositions of the materials collected from the four different DGI collection substrates. The analysis is carried out by means of a Zeiss MA EVO10 scanning electron microscope, equipped with a 10 mm^2 active area INCA X-act silicon-drift detector (Oxford Instruments). For each powder sample, five areas of approximatively 300 x 200 µm are analyzed, with an acquisition time of 500 s and a beam intensity of 300 pA. The elemental concentrations obtained in each region of interest are statistically averaged in order to obtain final compositional results. The experimental emission spectra are acquired at the instrument's ideal working distance of 8.5 mm (gun to sample surface). The elemental composition is probed by back-scattered electrons (BSE) in order to maximize the interaction volume of the incident beam with the sample. Conversely, the SEM images are acquired by detection of secondary electrons (SE) in order to highlight the morphological features of the collected powders.

2.4. Raman Spectroscopy Analysis

Raman Spectroscopy (RS) is used in order to obtain some information on the phase composition of the collected emissions, *i.e.* on the compounds composing the nano-powders. Raman probe is chosen after carrying out X-Ray Diffraction (XRD) analysis, which resulted in the complete absence of diffraction signals even when investigating the material from the **S3** collection substrate (800 < d_{50} < 900 nm). In spite of being demonstrated in the recent literature [19, 20, 21, 22, 23] as a valuable tool for the characterization of the crystalline fraction of the PM_{10} emissions generated by brakes, in this context the XRD probe fails to provide significant analytical signals, most likely due to combination of the two following factors: *i)* the extremely limited amount of analyzed material; and *ii)* the mostly nanometric nature of the investigated samples. Raman analysis is carried out by the mean of the Horiba LabRAM HR, equipped with a solid-state laser source (λ = 473 nm). The laser power is set nominally to 12.5 mW, since higher power values were found to damage the samples, leaving burnt micro-area after the measurements. All the spectra are acquired with 50x objective, which was found to be best magnification in order to maximize the signal to noise ratio. The acquisition range is set in the range of 50-2000 cm^{-1}, while high intensity grating (600 gr mm^{-1}) is used to maximize the collected signal. For each spectrum, five acquisition integrations of 10 sec are merged together along the whole investigated frequency range.

3. Results

The obtained results are reported in the following paragraphs. As previously described, the morphology of the collected emissions are evaluated via SEM imaging, while their elemental composition is characterized by means of EDXS analysis. Finally, the phase composition is assessed via Raman Spectroscopy.

3.1. Weights of Collected Emissions

As reported in paragraph 2.2, in spite of all the strategies employed to maximize the amount of collected material, nanoparticle emissions deposited on the lower stages of the ELPI+ are found not to be sufficient for a reliable chemical characterization. In particular, only two of the lower five collection substrates exhibit collected material weights significantly different from zero at the five-digit analytical balance. Conversely, due to the significantly higher working flow, appreciable amounts of material is collected on the DGI collection substrates: **S4** = 0.67 mg; **S3** = 5.91 mg; **S2** = 4.71 mg; **S1** = 0.46 mg.

As reported previously, only a quarter of each substrate is used for the chemical analysis, while the remaining material is spared for future toxicological characterizations, as planned for the second half of the nPETS Project [11]. Table 2 summarizes the weights in function of the dimensional fractions of the collected materials, while Figure 1 reports a visual comparison of substrates from ELPI+ and DGI with similar dimensional ranges.

TABLE 1 Summary table of measured weights of nanoparticles emissions collected by the mean of ELPI+ and DGI instruments.

ELPI +			DGI		
Stage	**d50/µm**	**Mass/mg**	**Stage**	**d50/µm**	**Mass/mg**
S6	0.150	0.00	**S4**	2.10-2.20	0.67
S5	0.095	0.01	**S3**	0.80-0.90	5.91
S4	0.054	0.00	**S2**	0.40-0.45	4.71
S3	0.030	0.02	**S1**	0.13-0.15	0.46
S2	0.016	0.00			
S1	0.006	0.00			

FIGURE 1 Comparison of: **a)** ELPI+ **S6**; and **b)** DGI **S1** collection substrates after the performed emission test. The two reported substrates collect material with similar dimensional dispersions, centered at about 150 nm.

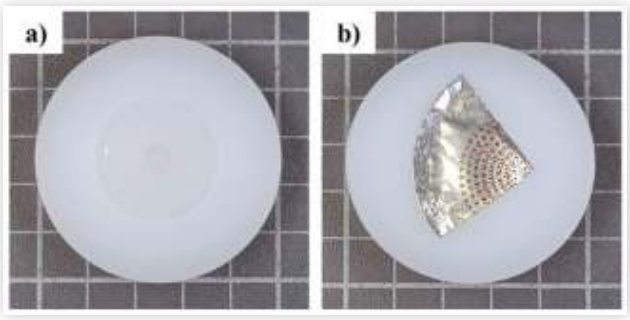

3.2. Particle Size Distribution Assessment

SEM images of the collected material are reported in Figure 2. The overall particle size distributions are coherent with the nominal d_{50} values expected as a function of the adopted flow rate, reported in Table 1. In particular, a progressive overall reduction in particle dimensions is apparent moving from **S4** to **S1**, with the material from the latter clearly exhibiting ultra-fine granulometry.

3.3. Elemental Composition

The elemental composition of the nanoparticle emission, in the form of the material collected on the DGI **S1** collection substrate, is investigated by means of EDXS analysis. In addition, the chemical composition of the material collected on the higher collection substrates from the DGI instrument (**S2**, **S3** and **S4**) is investigated for a comparative assessment with the ultra-fine fraction.

3.3.1. Substrate S1: 130 < d_{50} < 150 nm The elemental composition of the nanoparticle emission, in the form of the material collected on the DGI **S1** collection substrate (d_{50} < 150 nm), is investigated by means of EDXS analysis. Average elemental concentration values are reported in Table 2, together with the corresponding standard deviation over five independent observations. Figure 3 shows the elemental distributions over five different measurements, together with the average elemental composition, in the form of histograms.

The results reported in Table 2 and Figure 3 show that the elemental composition of the nanoparticle emission is dominated by the presence of three main elements, namely Iron, Carbon and Oxygen, as they account for over 85 wt% of the total particulate mass. Iron arises from both sides of the tribological interface, *i.e.* from the wear and tribo- oxidation of the cast iron and from the Iron-based compounds contained inside the friction mix.

In turn, Carbon is a more specific marker for the consumption of the friction material, since several Carbon-based compounds are common constituents of friction

FIGURE 2 Comparison of SEM images acquired on the collected material; from top to bottom: **a) S4**; **b) S3**; **c) S2**; and **d) S1** DGI collection substrates. **S4**: 2.1 < d_{50} < 2.2 m; **S3**: 800 < d_{50} < 900 nm; **S2**: 400 < d_{50} < 450 nm; **S1**: 130 < d_{50} < 150 nm.

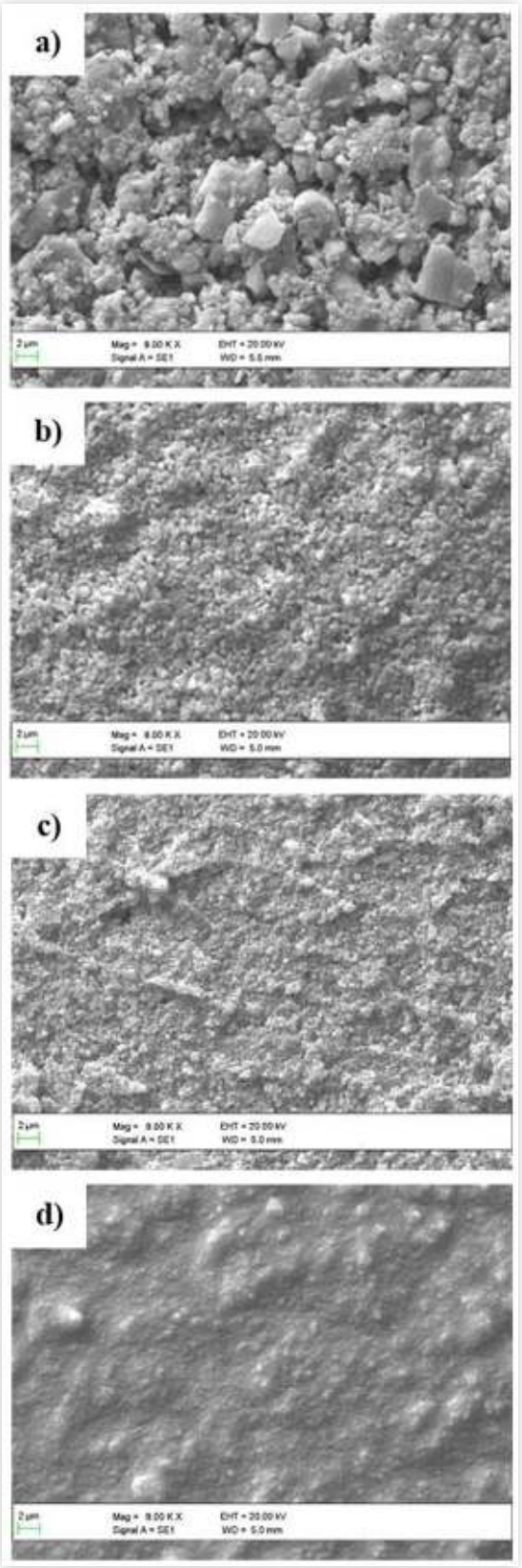

TABLE 2 Average elemental concentration values obtained for the nanoparticle emission collected on the DGI **S1** collection substrate. The standard deviation (SD) over five independent observations is reported for each element. Elements with concentrations lower than 0.1 wt% are not reported for brevity.

S1: 130 < d_{50} < 150 nm		
Element	**[wt%]**	**SD**
Fe	37.9	1.7
C	25.5	0.7
O	24.7	1.0
Sn	2.6	0.2
Zn	2.1	< 0.1
S	1.6	0.1
Mg	1.5	0.1
Si	1.4	< 0.1
Al	1.3	< 0.1
K	0.3	< 0.1
Mn	0.3	< 0.1
Cr	0.3	< 0.1
Cu	0.3	< 0.1
Others	*traces*	-

FIGURE 3 Distribution of elements as measured for the material collected on the DGI **S1** collection substrate: in the five independent observations (blue histograms) and averaged results (green histograms).

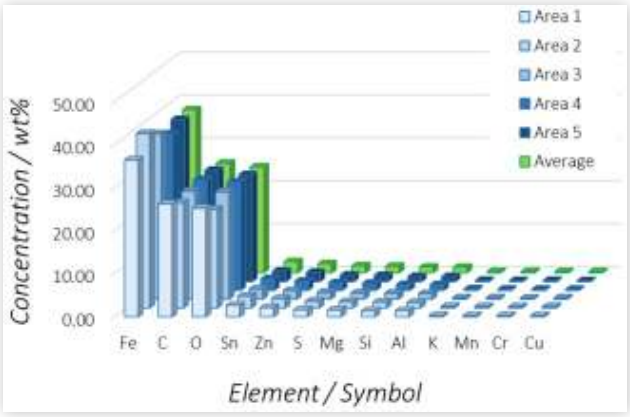

composites: organic resins as binders, graphite and cokes as solid lubricants, inorganic carbides and carbonates as abrasives and fillers [24]. However, a minor but not negligible contribution can also be ascribed to the wear of the cast iron braking disc, due to the presence of graphite lamellae within the Iron-based alloy. The Oxygen arises from both sides of the friction couple: it is indeed a marker for the oxidation of the metallic material from both the cast iron braking disc and the friction material, as well as for the inorganic oxides, carbonates and silicates commonly used in the friction mix as abrasives and fillers [24]. Finally, the nanoparticle emission features the minor presence of a set of secondary and trace elements, which are typically found in concentrations lower than 5 wt%. Together, these elements account for slightly more than 10 wt% of the total particulate mass. The presence of these elements relates closely to the specific friction material formulation and, secondary, to alloying elements of the worn cast iron.

3.3.2. Substrates S2-S4: 0.40 < d_{50} < 2.20 μm

The elemental composition of the emission collected on the higher DGI collection substrates (**S2** to **S4**), accounting for particulates with size distributions progressively shifted towards higher dimensions, are also reported for a comparative assessment with their ultra-fine counterpart. Overall average concentrations and corresponding standard deviations over five independent observations for each sample are showed in Table 3.

The comparison of the results shown in Table 3 reveals some statistically significant trends. In all the three materials deposited on the higher collection substrates there are three dominant elements, namely Iron, Oxygen and Carbon. Similarly to the case of the ultra-fine emission, these elements account for about 85 wt% of the total sample mass. However, their relative distribution changes moving towards the lower dimensional fractions. In particular, a constant decrease of the Iron concentration can be observed, while that of Oxygen remains constant. In addition, the Carbon concentration increases strongly moving from particulates with higher dimensions to their counterparts with lower dimensions, while the overall variation of the secondary and trace elements is modest. Figure 4 reports a graphical comparison of the average concentration values for the three main elements along the different dimensional ranges. Figure 5 summarizes the global situation for the sum of all the identified secondary and trace elements, while Figure 6 reports single contributions for each secondary element with an average concentration higher than 0.5 wt% to enable a more insightful discussion. Looking at the histogram reported in Figure 6 and comparing

TABLE 3 Average elemental concentration values obtained for the nanoparticle emission collected on the DGI **S2**, **S3** and **S4** collection substrates. The standard deviation (SD) over five independent observations is reported for each element. Elements with concentration lower than 0.1 wt% are not reported for brevity.

	S4		**S3**		**S2**	
Element	**[wt%]**	**SD**	**[wt%]**	**SD**	**[wt%]**	**SD**
Fe	50.5	1.9	46.3	2.6	44.4	2.4
O	26.0	1.2	25.3	1.0	25.4	1.9
C	9.2	0.9	14.1	2.1	16.8	3.6
Si	4.1	0.2	1.7	0.1	1.5	0.1
Sn	2.1	0.1	3.0	0.2	2.8	0.1
Zn	1.7	0.1	2.5	0.2	2.5	0.1
Al	1.5	< 0.1	1.8	0.2	1.7	<0.1
Mg	1.1	< 0.1	2.2	0.2	1.9	<0.1
S	0.8	< 0.1	1.5	0.1	1.5	<0.1
K	0.6	< 0.1	0.3	<0.1	0.3	<0.1
Cr	0.5	< 0.1	0.5	<0.1	0.4	<0.1
Cu	0.5	< 0.1	0.3	<0.1	0.3	<0.1
Mn	0.3	< 0.1	0.4	<0.1	0.4	<0.1
Others	*traces*	-	*traces*	-	*traces*	-

FIGURE 4 Comparison of average concentration values for the three main elements along the four investigated dimensional distributions. Error bars indicate standard deviations as ±σ around the corresponding average values.

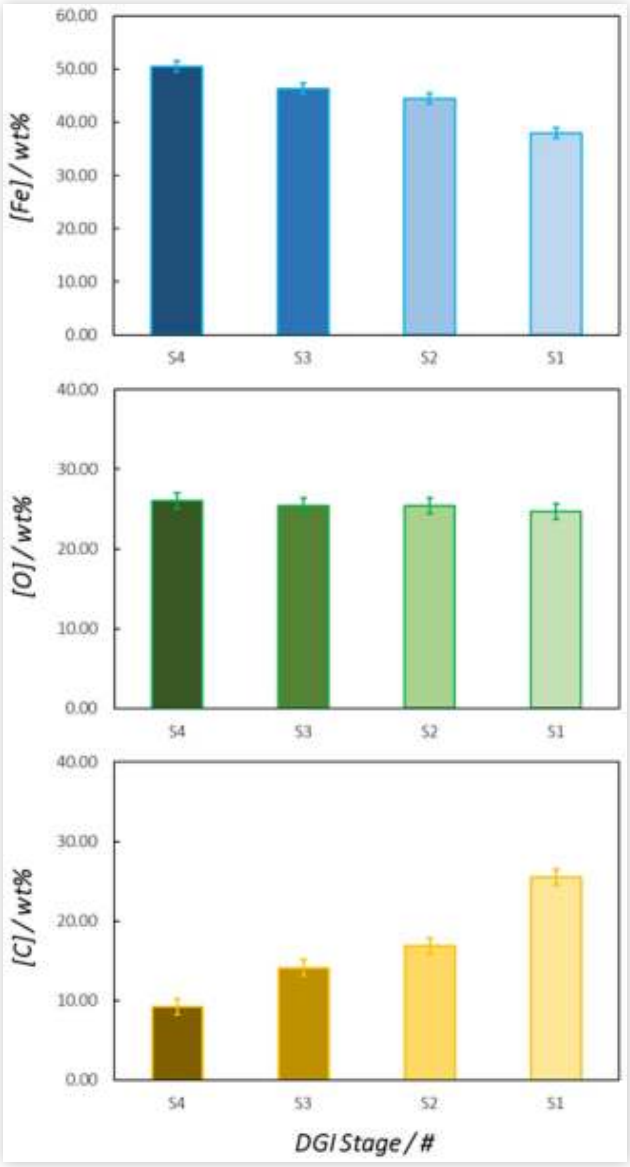

the values reported in Table 2 and 3, it is possible to notice that only Silicon preferentially segregates to the sample with the highest dimensional distribution, while all other elements show a limited decrease of average concentration moving from **S4** to **S1** (*i.e.*, from higher to lower overall particulate dimensions).

3.4. Phase Composition

Phase composition of the collected nanoparticle emissions is investigated via Raman Spectroscopy. Figure 7 shows the Raman spectrum acquired directly from the particulate obtained from the DGI **S1** collection substrate, together with the equivalent spectra collected from analyzing the materials sampled on the higher collection substrates (**S2**-**S4**). As can be observed, all the reported spectra look overall similar and

FIGURE 5 Comparison of average concentration values for secondary and trace elements along the four investigated dimensional distributions.

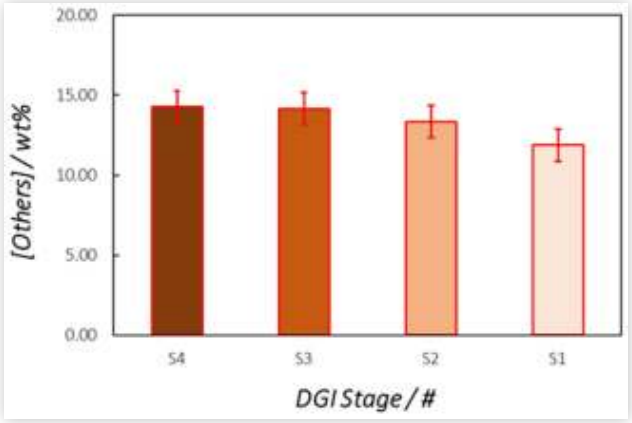

FIGURE 6 Detail of average concentration values for secondary elements (concentration > 0.5 wt%) along the four investigated dimensional distributions. Error bars indicates standard deviations as ±σ around the corresponding average values.

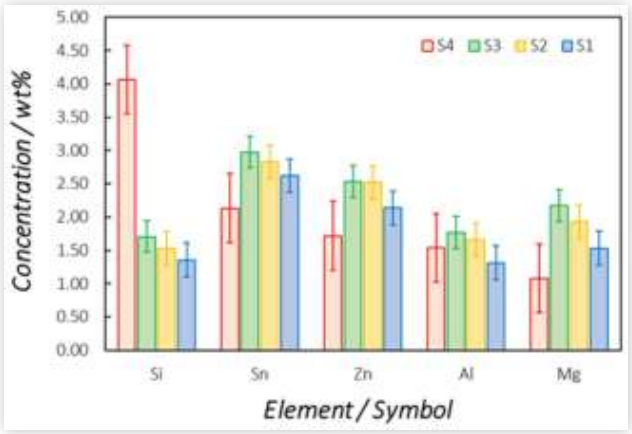

FIGURE 7 Comparison of Raman spectra acquired from the ultra-fine emission fraction (**S1**, green profile) and from coarser fractions (**S2** to **S4**, blue palette profiles).

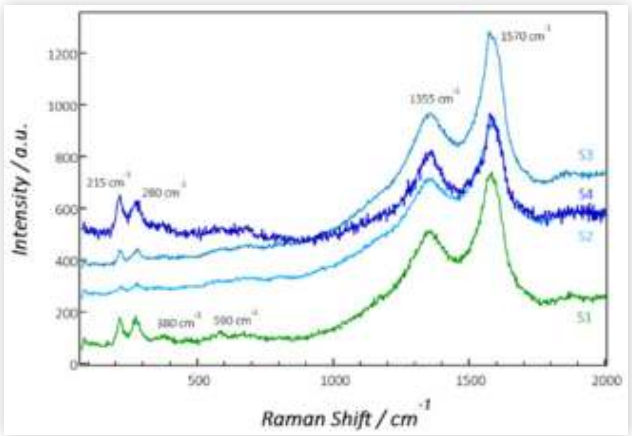

exhibit the same main features. In particular, two characteristic frequency ranges are apparent in all measured samples: *i)* the low frequencies, from 50 to 700 cm^{-1}, hosting signals from Iron oxides; and *ii)* the high frequencies, from 1200 to 2000 cm^{-1}, where signals from elemental Carbon typically reside. All the acquired spectra exhibit two peaks at about 215 and 280 cm^{-1}, which are associated with the Hematite (Fe_2O_3) phase. In the spectrum generated by the material collected on the **S1** collection substrate, it is also possible to recognize two additional broad features at about 380 and 590 cm^{-1} which are also coherent with the Hematite identification. Moving towards the higher frequencies, all spectra exhibit two peaks at about 1355 and 1570 cm^{-1}, which testify the presence of elemental Carbon (*i.e.,* graphites and cokes) inside the investigated particulates. All the described peaks are extremely broad and characterized by low intensities: this observation suggests an overall low degree of crystallinity of the identified compounds, which is coherent with the nature of the samples. Notably, the evaluation of the phase composition qualitatively confirms the trends observed in the elemental analysis. In particular, the intensity ratio between the peaks associated with Hematite and elemental Carbon is higher in the material collected on the **S4** substrate ($2.1 < d_{50} < 2.2$ µm), and decreases in the following stages. As far as the Iron/Oxygen ratio is concerned, it is possible to observe more defined characteristic features of the Hematite in the spectrum from the ultra-fine fraction (**S1**) with respect to its coarser counterparts: this observation is in good agreement with an overall higher degree of oxidation of the Iron, as already indicated by the elemental analysis results reported in the previous section.

4. Discussion

Considering all the results presented in this work, some interesting trends in the chemical composition of brakes emissions moving from the micrometric to the nanometric realm become apparent. In particular, at least two clear behaviors are identified: *i)* an overall decrease of the Iron/Oxygen ratio moving towards the ultra-fine particle dimensions; and *ii)* an overall increase of the Carbon-based material moving towards the lower particle size distributions.

Regarding the Fe/O ratio, it appears reasonable to expect an overall higher degree of oxidation in Iron particles with nanometric dimensions with respect to their counterparts of micrometric dimensions. This observation can be indeed well explained by considering the different specific areas generated by different particle size distributions. On the other hand, the increasing amount of Carbon-based material observed moving towards the nanoparticle emissions can be likely explained by considering the nature of the compounds which are typical sources of such element: organic resins as well as graphites and cokes are extremely brittle materials, which can generate exponential amounts of nanoparticles especially when exposed to increasing temperatures [25]. Notably, both trends presented here have been already reported and similarly discussed in the literature [19] when comparing the chemical composition of Debris material and PM_{10} emissions generated by a friction couple similar to the one used in this study (gray cast iron BD + ECE R90 Cu-Free and Low Steel FM). Also in that reference case [19], moving from coarser to finer granulometric profiles resulted in decreasing Iron/Oxygen ratio and increasing concentration of Carbon.

In addition to these main trends, other observational findings can be appreciated. Among the secondary and trace elements, only Silicon appears to be preferentially segregated in the highest dimensional fraction (**S4**): this can be likely explained by the specific granulometry and physical properties of its source compounds inside the friction mix. Conversely, all other elements are found in slightly higher concentrations in the lower dimensional size distributions (**S3**, **S2** and **S1**), with a general decreasing trend moving from sub-micrometric towards nanometric distributions.

5. Conclusions

This investigation reports for the first time a detailed study focused on the chemical characterization of nanoparticle emissions generated by brakes. In addition, a comparative assessment of both the elemental and phase composition of the ultra-fine emission fraction is reported with respect to its coarser counterparts. Furthermore, a wide discussion of the strategies adopted in order to overcome the intrinsic difficulties in collecting, manipulating and analyzing extremely limited amounts of nano-particulates is provided.

The reported elemental and phase analyses are in agreement in identifying two main compositional trends: *i)* a decreasing Iron/Oxygen ratio, *i.e.* a higher degree of Iron oxidation, when moving towards the finer fractions; and *ii)* a higher concentration of Carbon in the finer particulates. These findings suggest that, in spite of presenting overall similar compositional profiles in terms of constituent elements, particulates of different dimensional ranges exhibit significantly distinct elemental and phase compositions, mostly in terms of relative abundance of constituents compounds.

Therefore, it is possible to conclude that the chemical information arising from coarser brake emissions fractions should not be used when specifically assessing the ecological and toxicological behavior of nanoparticle emissions generated by the same source. Similar conclusion can be drawn for source apportionment studies targeting the accurate source determination of environmental nano-particulates.

References

1. World Health Organization, "WHO Air Quality Guidelines for Particulate Matter, Ozone, Nitrogen Dioxide and Sulfur Dioxide - Global Update 2005," Geneva, 2006.
2. European Environment Agency, "Air Quality in Europe - 2021 Report," Luxembourg, 2021.
3. European Council, "Directive 2008/50/EC," Bruxelles, 2008.
4. European Commission, "Commission Regulation (EU) N°459/2012," Bruxelles, 2012.

5. World Health Organization, "Burden of Disease from the Joint Effects of Household and Ambient Air Pollution for 2016," WHO, Geneva, 2018.
6. World Health Organization, "Economic Cost of the Health Impact of Air Pollution in Europe: Clean air, Health and Wealth," WHO, Geneva, 2015.
7. Pope, C.A., Burnett, R.T., Thun, M.J., Calle, E.E. et al., "Lung Cancer, Cardiopulmonary Mortality and Long-Term Exposure to Fine Particulate Air Pollution," *J. Am. Med. Assoc.* 287 (2002): 1132-1141.
8. Pope, C.A. and Dockery, D.D., "Health Effect of Fine Particulate Air Pollution: Lines that Connect," *J. Air Waste Manage. Assoc.* 56 (2002): 709-742.
9. Valavanidis, A., Fiotakis, K., and Vlachogianni, T., "Airborne Particulate Matter and Human Health: Toxicological Assessment and Importance of Size and Composition of Particles for Oxidative Damage and Carcirogenic Mechanisms," *J. Environ. Sci. and Health* 26, no. 4 (2008): 339-362.
10. Kim, K.H., Kabir, E., and Kabir, S., "A Review on the Human Health Impact of Airborne Particulate Matter," *Environ. Int.* 74 (2015): 136-143.
11. nPETS Project, "EU Horizon 2020's Research & Innovation Programme, Grant Agreement n°954377," 2020.
12. Pant, P. and Harrison, R.M., "Estimation of the Contribution of Road Traffic Emissions to Particulate Matter Concentrations from Field Measurements: A Review," *Atmos. Environ.* 77 (2013): 78-97.
13. Suleiman, A., Tight, M.R., and Quinn, A.D., "Assessment and Prediction of the Impact of Road Transport on Ambient Concentrations of Particulate Matter PM10," *Transp. Res. Part D* 49 (2016): 301-312.
14. Grigoratos, T. and Martini, G., "Brake Wear Particle Emissions: A Review," *Environ. Sci. Pollut. Res.* 22 (2015): 2491-2504.
15. Perricone, G., Wahlstrom, J., and Olofsson, U., "Towards a Test Stand for Standardized Measurements of the Brake Emissions," *Proc. I. Mech. E., Part D: J. Automobile Engineering* (2015): 1-8.
16. Perricone, G., Alemani, M., Metinoz, I., Matejka, V. et al., "Towards the Ranking of Airborne Particle Emissions from car Brakes - A System Approach," *Proc. I. Mech. E., Part D: J. Automobile Engineering* (2016): 1-17.
17. Mathissen, M., Grochowicz, J., Schmidt, C., Vogt, R. et al., "A novel Real-World Braking Cycle for Studying Brake Wear Emissions," *Wear* 414-415 (2018): 219-226.
18. Particle Measurement Programme Informal Working Group, "Informal Document GRPE_81_12, 81st GRPE," Agenda Item 7, June 9-11, 2020.
19. Mancini, A., Tsyupa, B., Pin, S., Bertasi, F. et al., "Novel Approaches for Physico-Chemical Characterization of Brake Emissions," EuroBrake2021 Technical Paper, EB2020-EBS-031, 2021.
20. Mancini, A., Tsyupa, B., Pin, S., Bandiera, M. et al., "Chemistry of the Brake Emissions: Influence of the Test Cycle," SAE Technical Paper 2021-01-1300, 2021, https://doi.org/10.4271/2021-01-1300.
21. Menapace, C., Mancini, A., Federici, M., Straffelini, G. et al., "Characterization of Airborne Wear Debris Produced by Brake Pads Pressed Against HVOF-Coated Discs," *Friction* 8, no. 2 (2020): 421-432.
22. Tsyupa, B., Federici, M., Bonfanti, A., Ansaloni, S. et al., "Reproducibility of Brake Emissions Chemical Composition: A First Inter-Laboratory Assessment," EuroBrake2022 Technical Paper, EB2022-EBS-019, 2022.
23. Tsyupa, B., Bandiera, M., Federici, M., Leonardi, M. et al., "Comparative Study of Size Distribution and Chemical Composition of Emissions from Low Steel and NAO Friction Materials," EuroBrake2022 Technical Paper, EB2022-EBS-021, 2022.
24. Dante, R.C., *Handbook of Friction Materials and Their Applications*, 1st ed. (Elsevier, The Woodhead Publishing, 2015)
25. Kukutschova, J. and Filip, P., *Non-Exhaust Emissions - Chapter 6: Review of Brake Wear Emissions* (Elsevier, 2018), 123-146.

Contact Information

Corresponding author: **Alessandro Mancini, PhD**
alessandro_mancini@brembo.it
O: +39 035 6052828
M: +39 346 0670785

Acknowledgments

Authors greatly thank *i)* all the colleagues involved in the design, the production and the testing of the braking discs and pads used for this research; and *ii)* the nPETS Project consortium.

ISSN 0148-7191